

Geophysical Research Letters[®]

RESEARCH LETTER

10.1029/2022GL100381

Special Section:

Atmospheric Rivers: Intersection of Weather and Climate

Key Points:

- Large differences in atmospheric river (AR) frequency and landfall in mid-latitudes depending on the Arctic stratospheric vortex strength
- Modulation occurs primarily through changes to tracks and decay regions of ARs with less change to genesis
- Stratospheric vortex modulation of ARs explains most of the associated seasonal-scale precipitation signal over Europe

Supporting Information:

Supporting Information may be found in the online version of this article.

Correspondence to:

S. H. Lee,
simon.h.lee@columbia.edu

Citation:


Lee, S. H., Polvani, L. M., & Guan, B. (2022). Modulation of atmospheric rivers by the Arctic stratospheric polar vortex. *Geophysical Research Letters*, 49, e2022GL100381. <https://doi.org/10.1029/2022GL100381>

Received 8 JUL 2022
Accepted 15 SEP 2022
Corrected 12 OCT 2022

This article was corrected on 12 OCT 2022. See the end of the full text for details.

© 2022. American Geophysical Union.
All Rights Reserved.

Modulation of Atmospheric Rivers by the Arctic Stratospheric Polar Vortex

Simon H. Lee¹ , Lorenzo M. Polvani^{1,2,3} , and Bin Guan^{4,5} 

¹Department of Applied Physics and Applied Mathematics, Columbia University, New York, NY, USA, ²Department of Earth and Environmental Sciences, Columbia University, New York, NY, USA, ³Lamont-Doherty Earth Observatory, Columbia University, Palisades, NY, USA, ⁴Jet Propulsion Laboratory, California Institute of Technology, Pasadena, CA, USA, ⁵Joint Institute for Regional Earth System Science and Engineering, University of California Los Angeles, Los Angeles, CA, USA

Abstract Variability in atmospheric river (AR) frequency can drive hydrometeorological extremes with broad societal impacts. Mitigating the impacts of increased or decreased AR frequency requires forewarning weeks to months ahead. A key driver of Northern Hemisphere wintertime mid-latitude subseasonal-to-seasonal climate variability is the stratospheric polar vortex. Here, we quantify AR frequency, landfall, genesis, and termination depending on the strength of the lower stratospheric polar vortex. We find large differences between weak and strong vortex states consistent with a latitudinal shift of the eddy-driven jet, with the greatest differences over the British Isles, Scandinavia, and Iberia. Significant differences are also found for the Pacific Northwest of North America. Most of the seasonal-scale stratospheric modulation of precipitation over Europe is explained by modulation of ARs. Our results provide potentially useful statistics for extended-range prediction, and highlight the importance of ARs in bringing about the precipitation response to anomalous vortex states.

Plain Language Summary Narrow bands of intense water vapor transport in the atmosphere, known as atmospheric rivers (ARs), can bring extreme rainfall to parts of the world, while their absence can lead to drought. So, it is important that we understand what aspects of the climate can affect their occurrence. During Northern Hemisphere winter, one of the key influences on weather patterns is the strength of the winds 10–50 km above the Arctic: the stratospheric polar vortex. These winds can persist in unusually weak or strong states for weeks to months at a time and influence the types of weather patterns we experience. We investigate changes to ARs depending on whether the vortex is weak or strong. We find large differences primarily across Europe but also parts of North America. We also find that ARs are important for bringing about changes to precipitation depending on the polar vortex strength. These results will help people plan for impacts from AR variability several weeks ahead, because the polar vortex usually remains weak or strong for several weeks at a time.

1. Introduction

Atmospheric rivers (ARs) are filamentary structures of intense horizontal water vapor transport usually located ahead of mid-latitude cyclone cold fronts (Ralph et al., 2018; Zhu & Newell, 1994). They contribute to over 90% of the meridional moisture transport across the mid-latitudes (Nash et al., 2018; Zhu & Newell, 1998) and play a dominant role in the hydroclimate of many regions of the world. Landfalling ARs can lead to extreme precipitation and flooding, particularly along the mountainous western coasts of North America and Europe owing to orographic uplift in addition to dynamic ascent within the AR (Corringham et al., 2019; Jennrich et al., 2020; Lavers & Villarini, 2013; Lavers et al., 2011, 2012; Rutz et al., 2014; Waliser & Guan, 2017). Additional impacts from landfalling ARs can include strong winds and unusual warmth (Waliser & Guan, 2017), while a deficit of ARs can lead to drought (Dettinger, 2013; Paltan et al., 2017).

A disproportionately large number of ARs are associated with climatic extremes (up to 50% of the top 2% of mid-latitude precipitation and wind events; Waliser & Guan, 2017) which emphasizes their direct relevance to significant societal impacts, in contrast to related phenomena such as extratropical cyclones. Although the “river” terminology is not new (Newell et al., 1992), ARs have received increased attention in recent years (Ralph et al., 2017), partly due to their popularity in the mainstream media and interdisciplinary science (Ralph et al., 2020) and their association with extreme rainfall in a warmer climate (Mahoney et al., 2018).

The diverse impacts associated with AR variability warrants sufficient forewarning to enable adequate preparedness, which may require probabilistic information at least several weeks ahead (White et al., 2017, 2022) where forecast skill is generally low. Characteristics of ARs, such as frequency, genesis and landfall probabilities, are influenced by large-scale modes of climate variability, which can also influence AR prediction skill (DeFlorio et al., 2018, 2019) or be leveraged to produce AR forecasts. Such modes of variability (which are not necessarily independent) include the El Niño-Southern Oscillation (H. Huang et al., 2021; Mundhenk et al., 2016; Payne & Magnusdottir, 2014; Zhou et al., 2021), the stratospheric Quasi-Biennial Oscillation (Baggett et al., 2017; Mundhenk et al., 2018), the Madden-Julian Oscillation (Baggett et al., 2017; Guan & Waliser, 2015; Guan et al., 2012; Toride & Hakim, 2021; Zhou et al., 2021), the Pacific-North American pattern (Guan & Waliser, 2015; Toride & Hakim, 2021), the Arctic/North Atlantic Oscillations (AO/NAO) (Benedict et al., 2019; Guan & Waliser, 2015), and regional weather regimes (Amini & Straus, 2019; Pasquier et al., 2019; Pohl et al., 2021).

However, to the best of our knowledge, the effect of the Arctic stratospheric polar vortex on ARs has not yet been quantified, despite its importance for mid-latitude subseasonal-to-seasonal (S2S) climate variability and predictability (Domeisen & Butler, 2020; Domeisen et al., 2020). Variability in vortex strength includes weak vortex events known as sudden stratospheric warmings (SSWs; e.g., Baldwin et al., 2021; Charlton & Polvani, 2007) and strong vortex events (e.g., Dunn-Sigouin & Shaw, 2015; Tripathi et al., 2015). The associated Northern Annular Mode (NAM) anomalies in the lower stratosphere, where the e -folding timescale is around 4 weeks (Baldwin et al., 2003; Simpson et al., 2011), can persist for at least 2 months (Baldwin & Dunkerton, 2001). This makes the stratosphere one of the most predictable components of the extratropical atmosphere (Son et al., 2020) and can provide a boundary condition for S2S forecasts (Charlton-Perez et al., 2021).

The tropospheric impacts of variability in stratospheric vortex strength include time-mean latitudinal shifts in the eddy-driven jets and mid-latitude storm tracks (Kidston et al., 2015; Kushner & Polvani, 2004; Maycock et al., 2020), shifts to the distribution and persistence of the AO/NAO concomitant with the stratospheric NAM anomaly (Ambaum & Hoskins, 2002; Baldwin & Dunkerton, 2001; Domeisen, 2019; Thompson et al., 2002), and modulation of recurrent flow regimes (Beerli & Grams, 2019; Charlton-Perez et al., 2018; Goss et al., 2021; Lee et al., 2019). Such tropospheric anomalies following the onset of anomalous vortex states are associated with distinct, and often extreme, mid-to-high latitude temperature and precipitation patterns (e.g., Douville, 2009; Goss et al., 2021; J. Huang et al., 2021; Knight et al., 2017; Kolstad et al., 2010; Zhang et al., 2022). The persistence of the stratospheric anomalies and the robust average tropospheric response can therefore yield “windows of opportunity” for actionable extended-range forecasts (Mariotti et al., 2020), which could be extended to include ARs.

In the present study, we quantify changes in AR frequency, landfall, genesis, and decay characteristics across the Northern Hemisphere depending on the strength of the lower-stratospheric vortex. Our results provide a foundation for improved extended-range predictions of ARs and better preparedness for impacts arising from AR variability.

2. Data and Methods

We use 6-hourly $0.5 \times 0.625^\circ$ data from the National Aeronautics and Space Administration (NASA) Modern-Era Retrospective analysis for Research and Applications version 2 (MERRA-2; Gelaro et al., 2017), considering all December–March (DJFM) days from 1 December 1980 to 31 March 2020 (excluding 29 February). We also repeated the analysis using 1.5° ERA-Interim data (Dee et al., 2011), finding negligible differences (not shown). DJFM is chosen as it features the largest variability in vortex strength (e.g., Baldwin et al., 2003). ARs are detected every 6 hr using the algorithm and MERRA-2 based data set of Guan and Waliser (2019). The globally consistent AR detection criteria used in this algorithm facilitate comparison across different regions. As the choice of AR data set can be a substantial source of uncertainty (e.g., Collow et al., 2022; Lora et al., 2020), we also repeat key analyses using the “Mundhenk v3” contribution (Mundhenk et al., 2016) to Tier 1 of the Atmospheric River Tracking Method Intercomparison Project (ARTMIP) (Rutz et al., 2019; Shields et al., 2018). The Mundhenk catalog is selected for comparison as it is based on a global percentile threshold, in contrast to the grid-point percentiles used by the Guan and Waliser algorithm (see also Ralph et al., 2019). In addition, it is among the closest to the ARTMIP Tier 1 median (Rutz et al., 2019) and we therefore consider it to be broadly representative of comparing the Guan and Waliser-based results with a multi-method ensemble.

To diagnose the strength of the lower-stratospheric vortex, we first compute the departure of the daily mean 100 hPa 60°N zonal-mean zonal winds (U100) from a 15-day centered average daily climatology over DJFM 1981–2020. We then classify the upper tercile of these anomalies ($>2.4 \text{ m s}^{-1}$) as a “strong vortex”, the middle tercile as a “neutral vortex”, and the lower tercile ($<-2.7 \text{ m s}^{-1}$) as a “weak vortex”, following Charlton-Perez et al. (2018). The daily classification of the vortex state is shown in Figure S1 in Supporting Information S1, where the characteristically long persistence of weak and strong vortex states is also evident. Because the average tropospheric circulation anomalies during neutral vortex conditions are minimal (Figure S2 in Supporting Information S1), we focus our analysis on weak and strong vortex states.

Statistical significance is assessed at the 95% confidence level. We employ a form of block-bootstrapping to test whether the results are likely to have arisen simply due to random structured sampling owing to the large auto-correlation of stratospheric vortex states. We randomly sample the population of DJFM days 10,000 times with the same structure as observed during each vortex state, by retaining the calendar day and month of each day within each season which is categorized into each tercile, and then shuffling the years. The observed sample is considered statistically significant if it lies outside the 2.5th and 97.5th percentiles of the synthetic distribution. In the seasonal-scale regression, the individual seasons are considered independent, and a simple bootstrap with replacement is performed against the null hypothesis of zero slope. In this case, the results are considered significant if zero lies outside the 2.5th–97.5th percentiles of the re-sampled slopes. In spatial maps, we account for multiple testing by employing the False Discovery Rate (FDR) correction following Wilks (2016), setting $\alpha_{\text{FDR}} = 0.1$.

3. AR Frequency

First, we analyze the grid-point frequency of AR conditions, defined as the average time each grid-point is contained within an AR shape boundary. Given the focus on subseasonal variability, we scale the results to the equivalent of “days per 4 weeks” (i.e., a value of 1 means a grid point is contained within an AR for an average of four not necessarily consecutive 6-hr time-steps in 28 days, or 3.6%). Figure 1a shows the climatological AR frequency for DJFM 1981–2020. The pink contour delineates regions where the frequency exceeds 3 days per 4 weeks—the largest integer number of days which intersects the western coastlines of North America and Europe. On average, AR conditions are common along almost the entire west coast of North America from northern California to Alaska, while in Europe only the British Isles experiences substantially frequent ARs (mostly due to the comparatively irregular coastline of Europe), consistent with previous studies (e.g., Guan & Waliser, 2015; Lavers et al., 2012; Neiman et al., 2008). ARs are also common along the eastern coast of North America and near the Persian Gulf.

We then compute the average AR frequency during weak vortex conditions (Figure 1b) and during strong vortex conditions (Figure 1c), alongside the respective percentage departures from climatology (Figures 1e and 1f). The largest differences are in the Atlantic, where the tropospheric response to anomalous vortex states is maximized via the NAO (Hitchcock & Simpson, 2014), but differences also exist across the Pacific-North America sector consistent with modulation of the AO/NAM.

When the vortex is weak (Figures 1b and 1e), ARs are on average shifted equatorward relative to climatology. In the Atlantic, the zone of highest Atlantic AR frequency (>3 days per 4 weeks) exhibits less meridional tilt compared with climatology, extending approximately along 30–35°N from Florida to Iberia, with a peak in the central subtropical Atlantic southwest of the Azores. This distribution is consistent with the structure of the “southern” eddy-driven jet regime (Woollings et al., 2010), which is favored following SSWs (Goss et al., 2021; Maycock et al., 2020). During a weak vortex, ARs are anomalously common in the Mediterranean (50% more common than climatology over southern Iberia), with a peak over Turkey exceeding 3 days per 4 weeks, consistent with increased precipitation and anomalous warmth in the Mediterranean following SSWs (Ayarzagüena et al., 2018; Domeisen & Butler, 2020; Monnin et al., 2021). ARs are much less likely across the British Isles and Scandinavia, where anomalies peak at -50% (Figure 1e). We also find a reduction in AR frequency near and west of British Columbia of around 20% during a weak vortex, consistent with the average easterly zonal wind anomalies in this region following SSWs (Afargan-Gerstman & Domeisen, 2020).

In contrast, during strong vortex conditions (Figures 1c and 1f), ARs are on average shifted poleward relative to climatology. The zone of highest AR frequency in the Atlantic exhibits a marked meridional tilt, extending

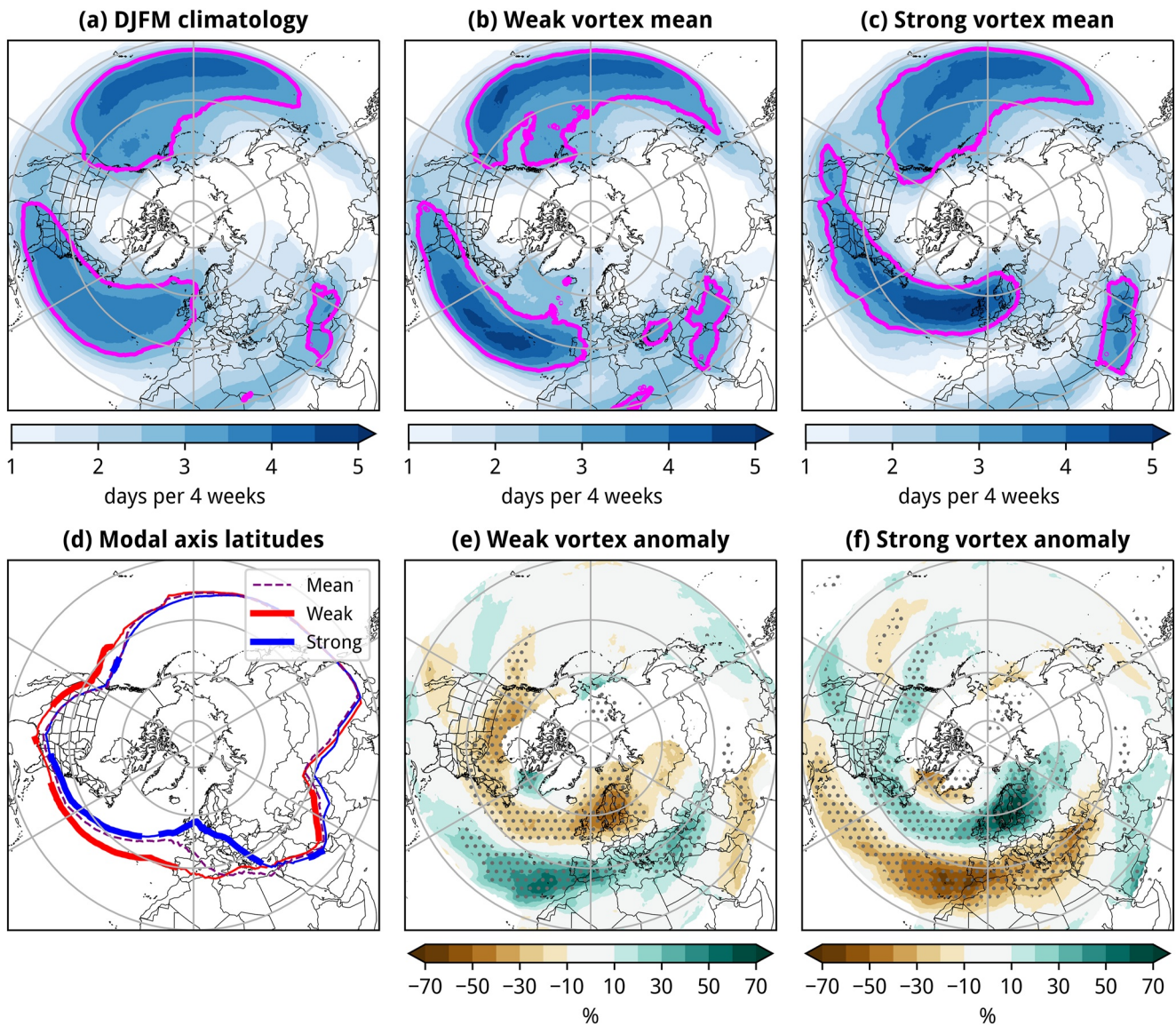


Figure 1. (a) Mean grid-point frequency of atmospheric river (AR) conditions over December–March (DJFM) 1981–2020, expressed as days per 4 weeks. The pink contour delineates a frequency of 3 days (i.e., twelve 6-hr time steps) per 4 weeks. Panel (b) as in panel (a) but averaged over all weak vortex days. Panel (c) as in panel (a) but averaged over all strong vortex days. (d) Modal latitudes of AR axes for each longitude, computed over centered 30° bins, during (red) weak and (blue) strong vortex conditions and (purple, dashed) DJFM climatology. Thick lines indicate significance at the 95% confidence level. (e) Percentage departure of the weak vortex mean AR frequency from climatology. Stippling denotes significance at the 95% confidence level (see Section 2 for details). Panel (f) as in panel (e) but for the strong vortex mean.

approximately from the Carolinas through the British Isles to Scandinavia, with increased zonal extent. This is consistent with the structure of the “northern” jet regime (Woollings et al., 2010), which is favored during strong vortex events (Goss et al., 2021). The combination of poleward shift and increased zonal extent yields anomalies of up to 70% over Scandinavia (Figure 1f), accordant with the tendency for ARs to occur most often in this region during the positive NAO (Benedict et al., 2019). The peak AR frequency of >4.5 days per 4 weeks—the highest in the entire Northern Hemisphere—extends across Ireland and the northern UK, which is the highest frequency of AR conditions *anywhere* over land during either vortex state or climatology. This agrees with widespread flooding in the UK during strong vortex winters (Davies et al., 2021; Knight et al., 2017). At the same time, ARs become very rare over Iberia and the Mediterranean during strong vortex conditions: anomalies reach up to -60% yielding an average frequency of <1 day per 4 weeks over southern Iberia and Morocco, consistent with the occurrence of drought during strong vortex winters such as 2019/2020 (Lawrence et al., 2020; NOAA, 2020)

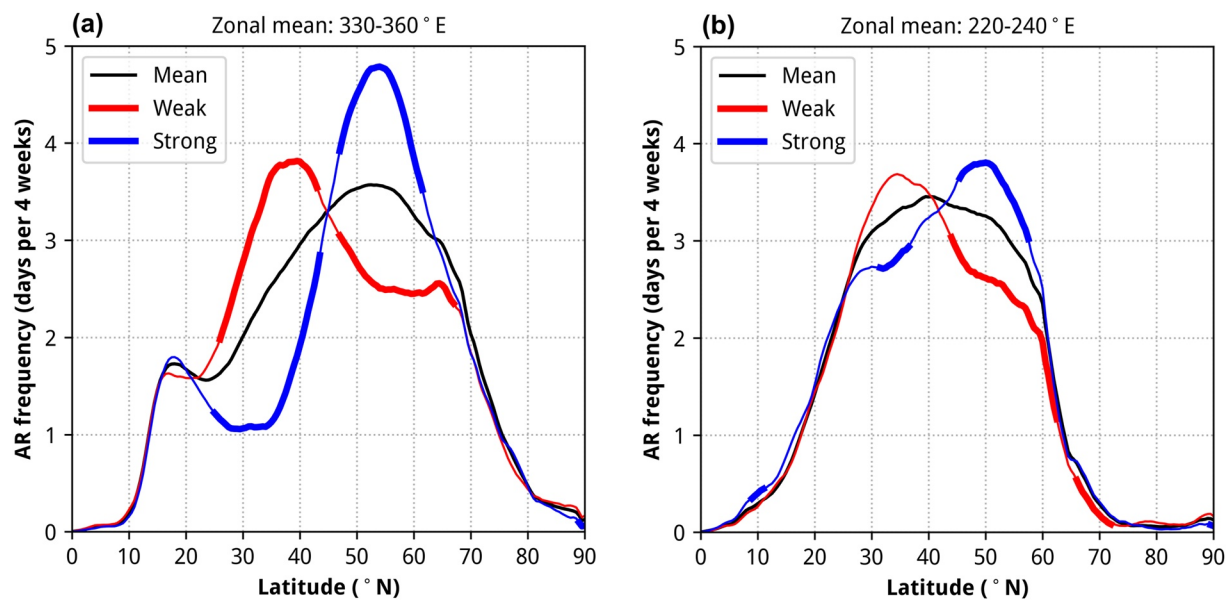


Figure 2. Zonal mean cross-sections of average atmospheric river frequency during strong (blue) and weak (red) vortex conditions for (a) the eastern North Atlantic, 330–360°E and (b) the eastern North Pacific, 220–240°E. Thick lines indicate the average is significantly different from that obtained by random sampling (see Section 2 for details).

and 2021/2022 (NOAA, 2022). And finally, we find a 10%–20% increase in AR frequency over British Columbia, with increased inland penetration.

Similar results to grid-point frequency are obtained using the modal latitude of AR axes (Figure 1d), where the axis is primarily defined by the maximum integrated vapor transport along the AR (see Guan and Waliser (2015)) and can thus be interpreted similarly to a cyclone track diagnostic. The modal axes are well-separated in the eastern North Atlantic. When the vortex is strong, AR axes typically intersect western Scotland toward southern Norway with a substantial poleward tilt. In contrast, when the vortex is weak, AR axes typically intersect Iberia with less tilt. Along the western coast of North America, the separation reaches $\sim 7^\circ$, corresponding to a shift from northern California when the vortex is weak to Washington when the vortex is strong. This is similar to the average cyclone tracks following weak and strong vortex events (Baldwin & Dunkerton, 2001) but further south.

To further illuminate the meridional structure of the frequency differences, we show latitudinal cross-sections of AR frequency in Figure 2, for the eastern Atlantic and eastern Pacific. In the Atlantic (Figure 2a) during strong vortex conditions, we find a double-peak structure (close to 20 and 55°N, with a local minimum near 30°N) consistent with well-separated subtropical and eddy-driven jets during the northern jet regime (Woollings et al., 2010). In contrast, during weak vortex conditions, AR frequency peaks close to 35°N, and the overall distribution is much broader. The departures from climatology during weak and strong vortex conditions are approximately equal and opposite. This effect results in ARs remaining relatively common near their climatological peak at $\sim 50^\circ\text{N}$ when the vortex is weak, whilst they become very infrequent near 35°N when the vortex is strong (i.e., close to southern Iberia). The larger, narrower peak during strong vortex conditions suggests a more meridionally constrained track of ARs, in agreement with the behavior of a zonally strengthened jet (Woollings et al., 2018) typical of the positive NAO.

For the Pacific (Figure 2b), only the anomalies poleward of 40°N are significant during both weak and strong vortex states. They are much smaller than for the Atlantic, although sufficient to shift the peak frequency from $\sim 35^\circ\text{N}$ when the vortex is weak to $\sim 50^\circ\text{N}$ when the vortex is strong—consistent with the modal axis latitudes in Figure 1d. As is the case in the Atlantic, the departures from climatology are approximately equal and opposite for both vortex states.

Equivalent analysis using the Mundhenk AR catalog can be found in Figures S3 and S4 in Supporting Information S1. Whilst some small differences exist, mainly due to differences in the climatological AR frequency (see also Rutz et al. (2019)), the primary results obtained using the Guan and Waliser catalog are unchanged. We can therefore be confident that our main conclusions are likely to be robust the choice of AR detection algorithm.

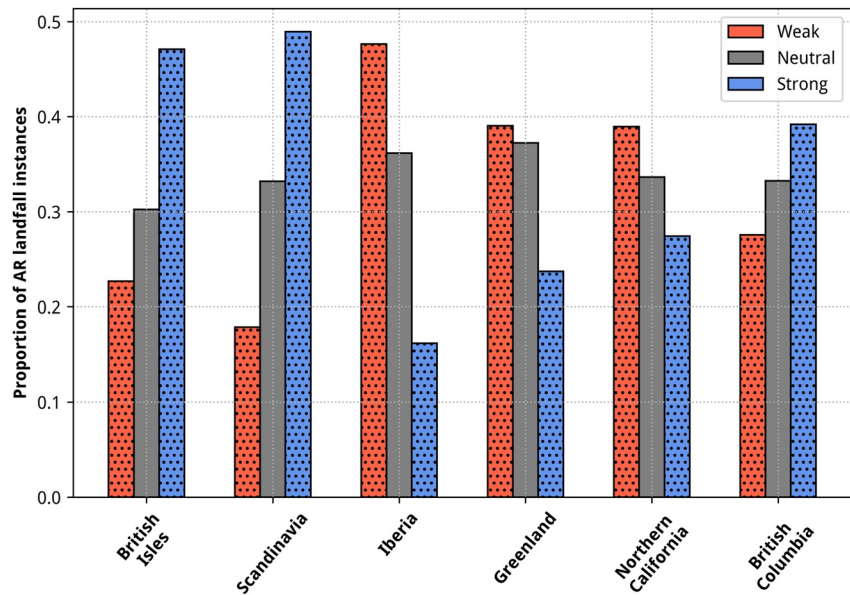


Figure 3. Proportion of atmospheric river landfalls occurring during weak (red), neutral (gray), and strong (blue) vortex conditions in grid-boxes covering the British Isles (50–60°N, 0–10°W), Scandinavia (55–70°N, 4–20°E), Iberia (36–44°N, 1–10°W), Greenland (59–70°N, 25–58°W), northern California (35–42°N, 125–120°W), and British Columbia (49–60°N, 120–140°W). Stippling indicates the proportion is significantly different from that obtained by random sampling (see Section 2 for details).

4. AR Landfall

We next assess the proportion of AR landfalls occurring during each vortex state for six key regions motivated by the preceding spatial analysis: the British Isles, Scandinavia, Iberia, Greenland, northern California, and British Columbia (a map of these regions is shown in Figure S5 in Supporting Information S1). AR landfall is defined for ARs moving from major oceans to major landmasses following Guan and Waliser (2015). Note that landfall can be defined for all time steps for which the same AR intersects the coastline, provided the mean integrated vapor transport is directed onshore and the remaining AR length over the ocean is >1,000 km.

As shown in Figure 3, almost 50% of AR landfalls in Scandinavia and the British Isles occur when the vortex is strong, approximately equal-and-opposite to landfalls in Iberia where nearly 50% occur when the vortex is weak. Only ~15%–17% of AR landfalls in Scandinavia occur during a weak vortex and in Iberia during a strong vortex. This highlights a large skew in the climatology with consequences for impacts from the attendant precipitation anomalies: approximately one-third of the time and often for extended periods of time due to the long stratospheric timescale, and AR landfalls are *much* more or *much* less common than average depending on the vortex state. The difference between strong and weak vortex states is greatest for Scandinavia, likely due to the aforementioned combined effect of the latitudinal shift, increased zonal extent, and more focused distribution of ARs when the vortex is strong. As suggested by Figures 1e and 1f, there are also changes to the probability of AR landfall on Greenland—where they significantly impact ice sheet mass balance (Mattingly et al., 2018)—with a marked reduction when the vortex is strong and a slight increase when the vortex is weak.

Differences between the proportion of AR landfalls occurring during each vortex state for Northern California and British Columbia are almost exactly opposing for the two regions. However, the overall changes are more muted in comparison with regions in the Atlantic sector (consistent with Figure 1).

5. AR Genesis and Decay

We now consider changes to AR genesis and decay during different vortex states (Figure 4) in order to further understand how the stratospheric vortex strength modulates AR frequencies.

AR genesis (Figures 4a–4c) is more frequent west of Iberia and in the Mediterranean when the vortex is weak versus strong, in agreement with the two distinct peaks in Mediterranean AR frequency during weak vortex states (Figure 1b).

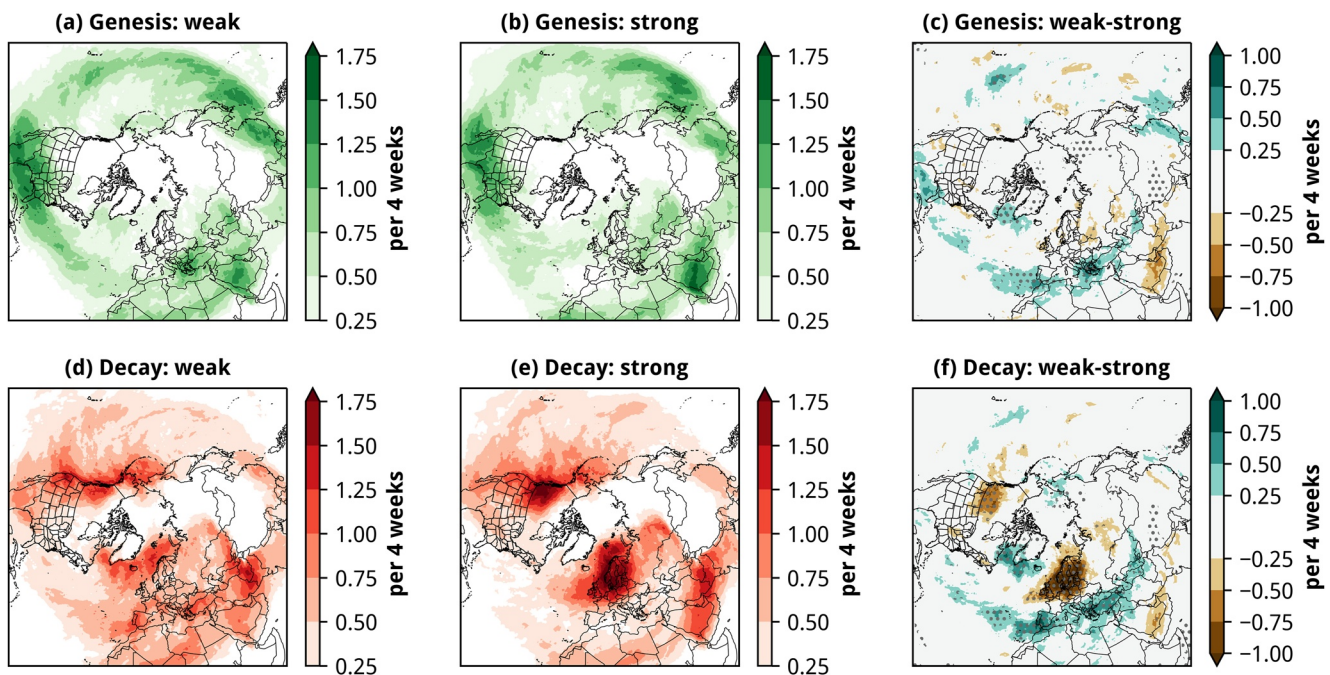


Figure 4. Average frequency of atmospheric river (AR) genesis (expressed in terms of occurrences per 4 weeks) during (a) weak and (b) strong vortex conditions, (c) and their difference. Panels (d–f) as in panels (a–c) but for AR decay frequency. Stippling in panels (c and f) indicates the difference is significantly different from random sampling (see Section 2 for details). Values below 0.25 (equivalent to 1 AR per 16 weeks) are not shown.

This indicates the eastern peak arises due to increased in situ genesis, rather than simply enhanced eastward propagation. We also note increased genesis near the southern tip of Greenland, consistent with the anomalously high AR frequency when the vortex is weak (Figure 1e). There is little indication of any change to AR genesis in the northeast Atlantic, the Pacific, or in subtropical regions where AR genesis is most common (e.g., Guan & Waliser, 2019).

Differences in AR decay probabilities between weak and strong vortex states (Figures 4d–4f) are generally larger than for genesis, except for the Mediterranean and west of Iberia where they are similar. AR decay is much more likely across the British Isles and Scandinavia when the vortex is strong. Because this region does not see markedly increased AR genesis during strong vortex conditions, both the increased AR frequency and decay is almost entirely due to shifts to AR tracks.

The shape of the maximum in decay probabilities over northwest Europe during strong vortex conditions resembles “Scandinavian blocking” and related patterns (e.g., Beerli & Grams, 2019; Cassou, 2008; Lee et al., 2020) and a region of frequent anticyclonic wave breaking (Masato et al., 2012), suggesting AR decay over northwest Europe during strong vortex conditions may be related to these processes. Thus, ARs may play a role in the relatively poor and resolution-dependent representation of variability in this region in S2S models (Büeler et al., 2021; Lee et al., 2020; Quinting & Vitart, 2019), given that low-resolution models may not fully resolve the filamentary nature of ARs or associated diabatic effects.

We also find a zone of increased AR decay in British Columbia during strong vortex conditions, consistent with the increased frequency and inland penetration of ARs in this region. Alongside the maximum in northwest Europe, these regions form “graveyards” of high AR decay frequency during strong vortex conditions. This contrasts with the more diffuse pattern during weak vortex conditions and suggests less track variability, consistent with a more zonally coherent jet.

6. Contribution to Precipitation Modulation by the Stratosphere

We finally assess the extent to which stratospheric modulation of ARs contributes to the stratospheric modulation of precipitation on the seasonal scale. We focus on Europe, where the seasonal-scale correlation between vortex strength and ARs is greatest (Figure S6 in Supporting Information S1).

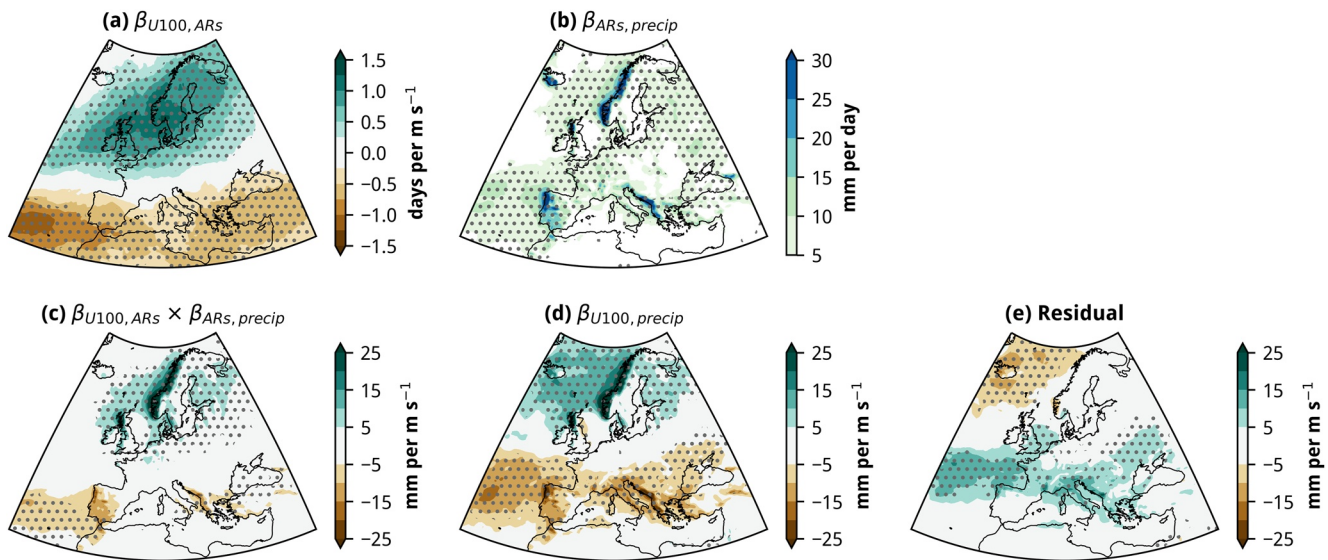


Figure 5. (a) Regression of December–March (DJFM)-mean U100 with DJFM-total atmospheric river (AR) frequency. (b) Regression of DJFM-total AR frequency with total precipitation. (c) Modulation of DJFM-total precipitation linearly explained by stratospheric modulation of AR frequency (i.e., $a \times b$). (d) Regression of DJFM-mean U100 with DJFM-total precipitation. (e) Modulation of DJFM-total precipitation *not* linearly explained by stratospheric modulation of AR frequency (i.e., c–d). Stippling indicates the regression coefficient is significantly different from zero at the 95% confidence level (with False Discovery Rate correction) according to 10,000 bootstrap re-samples with replacement.

First, we regress DJFM-mean U100 with DJFM-total AR frequency at each grid-point (Figure 5a) to quantify the seasonal-scale relationship between vortex strength and ARs. This yields a similar pattern of variability to that shown in Figures 1e and 1f. Next, we regress DJFM-total AR frequency at each grid-point with DJFM-total precipitation (Figure 5b), to quantify the linear contribution by ARs to the seasonal total precipitation. We then multiply these two regression maps together to estimate the variability in DJFM-total precipitation linearly explained by the vortex strength via ARs (Figure 5c). This can then be contrasted with the regression map of DJFM-mean U100 with DJFM-total precipitation (Figure 5d), with the residual (Figures 5c and 5d) shown in Figure 5e. We note that Figures 5c and 5d resemble the patterns of precipitation variability associated with stratospheric vortex variability shown in previous studies (Büeler et al., 2020; Douville, 2009; Goss et al., 2021).

The residual is small or insignificant in most regions—especially over Scandinavia, Scotland, Iberia, and south-east Europe, where the relationship between ARs and total precipitation (Figure 5b), and between the vortex strength and total precipitation (Figure 5d), is largest. The only notable exceptions are over the Atlantic near Iceland, west of France, and over northern Italy; these are regions where ARs contribute relatively little to precipitation and there is little association between the vortex strength and ARs. Thus, we conclude that the majority of the seasonal-scale variability in precipitation over Europe explained by a linear fit to the strength of the lower-stratospheric vortex occurs through modulation of AR frequency. As such, ARs play a leading role in bringing about the precipitation response to anomalous vortex states.

7. Summary

We have shown that there exist large differences in AR frequency (Figures 1 and 2), landfall (Figure 3), and genesis and decay probabilities (Figure 4) depending on the strength of the Arctic lower stratospheric polar vortex. These differences are greatest not over the oceans, but over highly populated regions of Europe and, to a lesser extent, the Pacific Northwest of North America, where the interaction of ARs with orography maximizes their potential impact.

We have further shown that the modulation of winter precipitation over Europe by the stratosphere is almost entirely due to the modulation of ARs (Figure 5). Thus, ARs are important in mediating the precipitation response to anomalous vortex states on the seasonal scale. Although we have not explicitly assessed the stratospheric influence on ARs in a predictive capacity, it follows that the extended persistence of weak and strong vortex states

and their accompanying impact on the persistence and predictability of tropospheric weather patterns (Baldwin et al., 2003; Charlton-Perez et al., 2018; Domeisen et al., 2020) can be translated to S2S forewarning of anomalous AR frequency. This is deserving of further study, particularly following the onset of SSWs and strong vortex events in the mid-stratosphere.

The ability of weather and climate models to represent ARs is likely to be important in their ability to fully represent the impacts of anomalous vortex states. Similarly, the ability of models to represent the tropospheric response to anomalous vortex states, especially variability in the North Atlantic eddy-driven jet which models have struggled to simulate correctly (e.g., Anstey et al., 2013), will be key to a faithful representation of the impact of the stratospheric vortex on ARs.

Data Availability Statement

NASA MERRA-2 data are available from the NASA Goddard Earth Sciences Data and Information Services Center at <https://disc.gsfc.nasa.gov/datasets?keywords=MERRA-2>. The Guan and Waliser AR data set (v3.0) is available from <https://ucla.app.box.com/v/ARcatalog>. The Mundhenk v3 AR data set is available from the Tier 1 ARTMIP database at <https://doi.org/10.5065/D6R78D1M>.

References

- Afargan-Gerstman, H., & Domeisen, D. I. (2020). Pacific modulation of the North Atlantic storm track response to sudden stratospheric warming events. *Geophysical Research Letters*, 47(2), e2019GL085007. <https://doi.org/10.1029/2019GL085007>
- Ambaum, M. H., & Hoskins, B. J. (2002). The NAO troposphere–stratosphere connection. *Journal of Climate*, 15(14), 1969–1978. [https://doi.org/10.1175/1520-0442\(2002\)015<1969:TNTSC>2.0.CO;2](https://doi.org/10.1175/1520-0442(2002)015<1969:TNTSC>2.0.CO;2)
- Amini, S., & Straus, D. M. (2019). Control of storminess over the Pacific and North America by circulation regimes. *Climate Dynamics*, 52(7), 4749–4770. <https://doi.org/10.1007/s00382-018-4409-7>
- Anstey, J. A., Davini, P., Gray, L. J., Woollings, T. J., Butchart, N., Cagnazzo, C., et al. (2013). Multi-model analysis of Northern Hemisphere winter blocking: Model biases and the role of resolution. *Journal of Geophysical Research: Atmospheres*, 118(10), 3956–3971. <https://doi.org/10.1002/jgd.50231>
- Ayarzagüena, B., Barriopedro, D., Garrido-Perez, J. M., Abalos, M., de la Cámara, A., García-Herrera, R., et al. (2018). Stratospheric connection to the abrupt end of the 2016/2017 Iberian drought. *Geophysical Research Letters*, 45(22), 12–639. <https://doi.org/10.1029/2018GL079802>
- Baggett, C. F., Barnes, E. A., Maloney, E. D., & Mundhenk, B. D. (2017). Advancing atmospheric river forecasts into subseasonal-to-seasonal time scales. *Geophysical Research Letters*, 44(14), 7528–7536. <https://doi.org/10.1002/2017GL074434>
- Baldwin, M. P., Ayarzagüena, B., Birner, T., Butchart, N., Butler, A. H., Charlton-Perez, A. J., et al. (2021). Sudden stratospheric warmings. *Reviews of Geophysics*, 59(1), e2020RG000708. <https://doi.org/10.1029/2020RG000708>
- Baldwin, M. P., & Dunkerton, T. J. (2001). Stratospheric harbingers of anomalous weather regimes. *Science*, 294(5542), 581–584. <https://doi.org/10.1126/science.1063315>
- Baldwin, M. P., Stephenson, D. B., Thompson, D. W., Dunkerton, T. J., Charlton, A. J., & O'Neill, A. (2003). Stratospheric memory and skill of extended-range weather forecasts. *Science*, 301(5633), 636–640. <https://doi.org/10.1126/science.1087143>
- Beerli, R., & Grams, C. M. (2019). Stratospheric modulation of the large-scale circulation in the Atlantic–European region and its implications for surface weather events. *Quarterly Journal of the Royal Meteorological Society*, 145(725), 3732–3750. <https://doi.org/10.1002/qj.3653>
- Benedict, I., Ødemark, K., Nipen, T., & Moore, R. (2019). Large-scale flow patterns associated with extreme precipitation and atmospheric rivers over Norway. *Monthly Weather Review*, 147(4), 1415–1428. <https://doi.org/10.1175/MWR-D-18-0362.1>
- Büeler, D., Beerli, R., Wernli, H., & Grams, C. M. (2020). Stratospheric influence on ECMWF sub-seasonal forecast skill for energy-industry-relevant surface weather in European countries. *Quarterly Journal of the Royal Meteorological Society*, 146(733), 3675–3694. <https://doi.org/10.1002/qj.3866>
- Büeler, D., Ferranti, L., Magnusson, L., Quinting, J. F., & Grams, C. M. (2021). Year-round sub-seasonal forecast skill for Atlantic–European weather regimes. *Quarterly Journal of the Royal Meteorological Society*, 147(741), 4283–4309. <https://doi.org/10.1002/qj.4178>
- Cassou, C. (2008). Intraseasonal interaction between the Madden–Julian oscillation and the North Atlantic oscillation. *Nature*, 455(7212), 523–527. <https://doi.org/10.1038/nature07286>
- Charlton, A. J., & Polvani, L. M. (2007). A new look at stratospheric sudden warmings. Part I: Climatology and modeling benchmarks. *Journal of Climate*, 20(3), 449–469. <https://doi.org/10.1175/JCLI3996.1>
- Charlton-Perez, A. J., Bröcker, J., Karpechko, A. Y., Lee, S. H., Sigmond, M., & Simpson, I. R. (2021). A minimal model to diagnose the contribution of the stratosphere to tropospheric forecast skill. *Journal of Geophysical Research: Atmospheres*, 126(24), e2021JD035504. <https://doi.org/10.1029/2021JD035504>
- Charlton-Perez, A. J., Ferranti, L., & Lee, R. W. (2018). The influence of the stratospheric state on North Atlantic weather regimes. *Quarterly Journal of the Royal Meteorological Society*, 144(713), 1140–1151. <https://doi.org/10.1002/qj.3280>
- Collow, A. M., Shields, C. A., Guan, B., Kim, S., Lora, J., McClenney, E., et al. (2022). An overview of ARTMIP's Tier 2 reanalysis intercomparison: Uncertainty in the detection of atmospheric rivers and their associated precipitation. *Journal of Geophysical Research: Atmospheres*, 127(8), e2021JD036155. <https://doi.org/10.1029/2021JD036155>
- Corringham, T. W., Ralph, F. M., Gershunov, A., Cayan, D. R., & Talbot, C. A. (2019). Atmospheric rivers drive flood damages in the western United States. *Science Advances*, 5(12), eaax4631. <https://doi.org/10.1126/sciadv.aax4631>
- Davies, P. A., McCarthy, M., Christidis, N., Dunstone, N., Fereday, D., Kendon, M., et al. (2021). The wet and stormy UK winter of 2019/2020. *Weather*, 76(12), 396–402. <https://doi.org/10.1002/wea.3955>
- Dee, D. P., Uppala, S. M., Simmons, A. J., Berrisford, P., Poli, P., Kobayashi, S., et al. (2011). The ERA-Interim reanalysis: Configuration and performance of the data assimilation system. *Quarterly Journal of the Royal Meteorological Society*, 137(656), 553–597. <https://doi.org/10.1002/qj.828>

Acknowledgments

S.H.L. and L.M.P. acknowledge funding from National Science Foundation grant AGS-1914569 to Columbia University. B.G. acknowledges funding from the California Department of Water Resources Atmospheric Rivers Program via University of California, San Diego, and from NASA Grant 80NSSC22K0926. All analyses were performed on the Ginsburg HPC cluster at Columbia University. We acknowledge two anonymous reviewers for their helpful comments which improved the paper.

- DeFlorio, M. J., Waliser, D. E., Guan, B., Lavers, D. A., Ralph, F. M., & Vitart, F. (2018). Global assessment of atmospheric river prediction skill. *Journal of Hydrometeorology*, *19*(2), 409–426. <https://doi.org/10.1175/JHM-D-17-0135.1>
- DeFlorio, M. J., Waliser, D. E., Guan, B., Ralph, F. M., & Vitart, F. (2019). Global evaluation of atmospheric river subseasonal prediction skill. *Climate Dynamics*, *52*(5), 3039–3060. <https://doi.org/10.1007/s00382-018-4309-x>
- Dettinger, M. D. (2013). Atmospheric rivers as drought busters on the US West Coast. *Journal of Hydrometeorology*, *14*(6), 1721–1732. <https://doi.org/10.1175/JHM-D-13-02.1>
- Domeisen, D. I. (2019). Estimating the frequency of sudden stratospheric warming events from surface observations of the North Atlantic Oscillation. *Journal of Geophysical Research: Atmospheres*, *124*(6), 3180–3194. <https://doi.org/10.1029/2018JD030077>
- Domeisen, D. I., & Butler, A. H. (2020). Stratospheric drivers of extreme events at the Earth's surface. *Communications Earth & Environment*, *1*(1), 1–8. <https://doi.org/10.1038/s43247-020-00060-z>
- Domeisen, D. I., Butler, A. H., Charlton-Perez, A. J., Ayarzagüena, B., Baldwin, M. P., Dunn-Sigouin, E., et al. (2020). The role of the stratosphere in subseasonal to seasonal prediction: 2. Predictability arising from stratosphere-troposphere coupling. *Journal of Geophysical Research: Atmospheres*, *125*(2), e2019JD030923. <https://doi.org/10.1029/2019JD030923>
- Douville, H. (2009). Stratospheric polar vortex influence on Northern Hemisphere winter climate variability. *Geophysical Research Letters*, *36*(18), L18703. <https://doi.org/10.1029/2009GL039334>
- Dunn-Sigouin, E., & Shaw, T. A. (2015). Comparing and contrasting extreme stratospheric events, including their coupling to the tropospheric circulation. *Journal of Geophysical Research: Atmospheres*, *120*(4), 1374–1390. <https://doi.org/10.1002/2014JD022116>
- Gelaro, R., McCarty, W., Suárez, M. J., Todling, R., Molod, A., Takacs, L., et al. (2017). The modern-era retrospective analysis for research and applications, version 2 (MERRA-2). *Journal of Climate*, *30*(14), 5419–5454. <https://doi.org/10.1175/JCLI-D-16-0758.1>
- Goss, M., Lindgren, E. A., Sheshadri, A., & Diffenbaugh, N. S. (2021). The Atlantic jet response to stratospheric events: A regime perspective. *Journal of Geophysical Research: Atmospheres*, *126*(7), e2020JD033358. <https://doi.org/10.1029/2020JD033358>
- Guan, B., & Waliser, D. E. (2015). Detection of atmospheric rivers: Evaluation and application of an algorithm for global studies. *Journal of Geophysical Research: Atmospheres*, *120*(24), 12514–12535. <https://doi.org/10.1002/2015JD024257>
- Guan, B., & Waliser, D. E. (2019). Tracking atmospheric rivers globally: Spatial distributions and temporal evolution of life cycle characteristics. *Journal of Geophysical Research: Atmospheres*, *124*(23), 12523–12552. <https://doi.org/10.1029/2019JD031205>
- Guan, B., Waliser, D. E., Molotch, N. P., Fetzer, E. J., & Neiman, P. J. (2012). Does the Madden-Julian oscillation influence wintertime atmospheric rivers and snowpack in the Sierra Nevada? *Monthly Weather Review*, *140*(2), 325–342. <https://doi.org/10.1175/MWR-D-11-00087.1>
- Hitchcock, P., & Simpson, I. R. (2014). The downward influence of stratospheric sudden warmings. *Journal of the Atmospheric Sciences*, *71*(10), 3856–3876. <https://doi.org/10.1175/JAS-D-14-0012.1>
- Huang, H., Patricola, C. M., Bercos-Hickey, E., Zhou, Y., Rhoades, A., Risser, M. D., & Collins, W. D. (2021). Sources of subseasonal-to-seasonal predictability of atmospheric rivers and precipitation in the western United States. *Journal of Geophysical Research: Atmospheres*, *126*(6), e2020JD034053. <https://doi.org/10.1029/2020JD034053>
- Huang, J., Hitchcock, P., Maycock, A. C., McKenna, C. M., & Tian, W. (2021). Northern hemisphere cold air outbreaks are more likely to be severe during weak polar vortex conditions. *Communications Earth & Environment*, *2*(1), 1–11. <https://doi.org/10.1038/s43247-021-00215-6>
- Jennrich, G. C., Furtado, J. C., Basara, J. B., & Martin, E. R. (2020). Synoptic characteristics of 14-day extreme precipitation events across the United States. *Journal of Climate*, *33*(15), 6423–6440. <https://doi.org/10.1175/JCLI-D-19-0563.1>
- Kidston, J., Scaife, A. A., Hardiman, S. C., Mitchell, D. M., Butchart, N., Baldwin, M. P., & Gray, L. J. (2015). Stratospheric influence on tropospheric jet streams, storm tracks and surface weather. *Nature Geoscience*, *8*(6), 433–440. <https://doi.org/10.1038/ngeo2424>
- Knight, J. R., Maidens, A., Watson, P. A., Andrews, M., Belcher, S., Brunet, G., et al. (2017). Global meteorological influences on the record UK rainfall of winter 2013–14. *Environmental Research Letters*, *12*(7), 074001. <https://doi.org/10.1088/1748-9326/aa693c>
- Kolstad, E. W., Breiteig, T., & Scaife, A. A. (2010). The association between stratospheric weak polar vortex events and cold air outbreaks in the Northern Hemisphere. *Quarterly Journal of the Royal Meteorological Society*, *136*(649), 886–893. <https://doi.org/10.1002/qj.620>
- Kushner, P. J., & Polvani, L. M. (2004). Stratosphere–troposphere coupling in a relatively simple AGCM: The role of eddies. *Journal of Climate*, *17*(3), 629–639. [https://doi.org/10.1175/1520-0442\(2004\)017<0629:SCIARS>2.0.CO;2](https://doi.org/10.1175/1520-0442(2004)017<0629:SCIARS>2.0.CO;2)
- Lavers, D. A., Allan, R. P., Wood, E. F., Villarini, G., Brayshaw, D. J., & Wade, A. J. (2011). Winter floods in Britain are connected to atmospheric rivers. *Geophysical Research Letters*, *38*(23). <https://doi.org/10.1029/2011GL049783>
- Lavers, D. A., & Villarini, G. (2013). The nexus between atmospheric rivers and extreme precipitation across Europe. *Geophysical Research Letters*, *40*(12), 3259–3264. <https://doi.org/10.1002/grl.50636>
- Lavers, D. A., Villarini, G., Allan, R. P., Wood, E. F., & Wade, A. J. (2012). The detection of atmospheric rivers in atmospheric reanalyses and their links to British winter floods and the large-scale climatic circulation. *Journal of Geophysical Research*, *117*(D20), D201106. <https://doi.org/10.1029/2012JD018027>
- Lawrence, Z. D., Perlwitz, J., Butler, A. H., Manney, G. L., Newman, P. A., Lee, S. H., & Nash, E. R. (2020). The remarkably strong Arctic stratospheric polar vortex of winter 2020: Links to record-breaking Arctic oscillation and ozone loss. *Journal of Geophysical Research: Atmospheres*, *125*(22), e2020JD033271. <https://doi.org/10.1029/2020JD033271>
- Lee, S. H., Charlton-Perez, A. J., Furtado, J. C., & Woolnough, S. J. (2020). Representation of the Scandinavia–Greenland pattern and its relationship with the polar vortex in S2S forecast models. *Quarterly Journal of the Royal Meteorological Society*, *146*(733), 4083–4098. <https://doi.org/10.1002/qj.3892>
- Lee, S. H., Furtado, J. C., & Charlton-Perez, A. J. (2019). Wintertime North American weather regimes and the Arctic stratospheric polar vortex. *Geophysical Research Letters*, *46*(24), 14892–14900. <https://doi.org/10.1029/2019GL085592>
- Lora, J. M., Shields, C., & Rutz, J. (2020). Consensus and disagreement in atmospheric river detection: ARTMIP global catalogues. *Geophysical Research Letters*, *47*(20), e2020GL089302. <https://doi.org/10.1029/2020GL089302>
- Mahoney, K., Swales, D., Mueller, M. J., Alexander, M., Hughes, M., & Malloy, K. (2018). An examination of an inland-penetrating atmospheric river flood event under potential future thermodynamic conditions. *Journal of Climate*, *31*(16), 6281–6297. <https://doi.org/10.1175/JCLI-D-18-0118.1>
- Mariotti, A., Baggett, C., Barnes, E. A., Becker, E., Butler, A., Collins, D. C., et al. (2020). Windows of opportunity for skillful forecasts subseasonal to seasonal and beyond. *Bulletin of the American Meteorological Society*, *101*(5), E608–E625. <https://doi.org/10.1175/BAMS-D-18-0326.1>
- Masato, G., Hoskins, B., & Woollings, T. J. (2012). Wave-breaking characteristics of midlatitude blocking. *Quarterly Journal of the Royal Meteorological Society*, *138*(666), 1285–1296. <https://doi.org/10.1002/qj.990>
- Mattingly, K., Mote, T., & Fettweis, X. (2018). Atmospheric river impacts on Greenland Ice Sheet surface mass balance. *Journal of Geophysical Research: Atmospheres*, *123*(16), 8538–8560. <https://doi.org/10.1029/2018JD028714>
- Maycock, A. C., Masukwedza, G. I., Hitchcock, P., & Simpson, I. R. (2020). A regime perspective on the North Atlantic eddy-driven jet response to sudden stratospheric warmings. *Journal of Climate*, *33*(9), 3901–3917. <https://doi.org/10.1175/JCLI-D-19-0702.1>

- Monnin, E., Kretschmer, M., & Polichtchouk, I. (2021). The role of the timing of sudden stratospheric warmings for precipitation and temperature anomalies in Europe. *International Journal of Climatology*, 42(6), 3448–3462. <https://doi.org/10.1002/joc.7426>
- Mundhenk, B. D., Barnes, E. A., & Maloney, E. D. (2016). All-season climatology and variability of atmospheric river frequencies over the North Pacific. *Journal of Climate*, 29(13), 4885–4903. <https://doi.org/10.1175/JCLI-D-15-0665.1>
- Mundhenk, B. D., Barnes, E. A., Maloney, E. D., & Baggett, C. F. (2018). Skillful empirical subseasonal prediction of landfalling atmospheric river activity using the Madden–Julian oscillation and quasi-biennial oscillation. *NPJ Climate and Atmospheric Science*, 1(1), 1–7. <https://doi.org/10.1038/s41612-017-0008-2>
- Nash, D., Waliser, D., Guan, B., Ye, H., & Ralph, F. M. (2018). The role of atmospheric rivers in extratropical and polar hydroclimate. *Journal of Geophysical Research: Atmospheres*, 123(13), 6804–6821. <https://doi.org/10.1029/2017JD028130>
- Neiman, P. J., Ralph, F. M., Wick, G. A., Lundquist, J. D., & Dettinger, M. D. (2008). Meteorological characteristics and overland precipitation impacts of atmospheric rivers affecting the West Coast of North America based on eight years of SSM/I satellite observations. *Journal of Hydrometeorology*, 9(1), 22–47. <https://doi.org/10.1175/2007JHM855.1>
- Newell, R. E., Newell, N. E., Zhu, Y., & Scott, C. (1992). Tropospheric rivers?—A pilot study. *Geophysical Research Letters*, 19(24), 2401–2404. <https://doi.org/10.1029/92GL02916>
- NOAA. (2020). February 2020 global climate report: National Centers for Environmental Information. Retrieved from <https://www.ncei.noaa.gov/access/monitoring/monthly-report/global/202002>
- NOAA. (2022). February 2022 global climate report: National Centers for Environmental Information. Retrieved from <https://www.ncei.noaa.gov/access/monitoring/monthly-report/global/202202>
- Paltan, H., Waliser, D., Lim, W. H., Guan, B., Yamazaki, D., Pant, R., & Dadson, S. (2017). Global floods and water availability driven by atmospheric rivers. *Geophysical Research Letters*, 44(20), 10–387. <https://doi.org/10.1002/2017GL074882>
- Pasquier, J., Pfahl, S., & Grams, C. M. (2019). Modulation of atmospheric river occurrence and associated precipitation extremes in the North Atlantic region by European weather regimes. *Geophysical Research Letters*, 46(2), 1014–1023. <https://doi.org/10.1029/2018GL081194>
- Payne, A. E., & Magnusdottir, G. (2014). Dynamics of landfalling atmospheric rivers over the North Pacific in 30 years of MERRA reanalysis. *Journal of Climate*, 27(18), 7133–7150. <https://doi.org/10.1175/JCLI-D-14-00034.1>
- Pohl, B., Favier, V., Wille, J., Udy, D. G., Vance, T. R., Pergaud, J., et al. (2021). Relationship between weather regimes and atmospheric rivers in East Antarctica. *Journal of Geophysical Research: Atmospheres*, 126(24), e2021JD035294. <https://doi.org/10.1029/2021JD035294>
- Quinting, J., & Vitart, F. (2019). Representation of synoptic-scale Rossby wave packets and blocking in the S2S prediction project database. *Geophysical Research Letters*, 46(2), 1070–1078. <https://doi.org/10.1029/2018GL081381>
- Ralph, F. M., Dettinger, M., Lavers, D., Gorodetskaya, I. V., Martin, A., Viale, M., et al. (2017). Atmospheric rivers emerge as a global science and applications focus. *Bulletin of the American Meteorological Society*, 98(9), 1969–1973. <https://doi.org/10.1175/BAMS-D-16-0262.1>
- Ralph, F. M., Dettinger, M. D., Cairns, M. M., Galarneau, T. J., & Eylander, J. (2018). Defining “atmospheric river”: How the glossary of meteorology helped resolve a debate. *Bulletin of the American Meteorological Society*, 99(4), 837–839. <https://doi.org/10.1175/BAMS-D-17-0157.1>
- Ralph, F. M., Waliser, D. E., Dettinger, M. D., Rutz, J. J., Anderson, M. L., Gorodetskaya, I. V., et al. (2020). The future of atmospheric river research and applications. In *Atmospheric rivers* (pp. 219–247). Springer. https://doi.org/10.1007/978-3-030-28906-5_8
- Ralph, F. M., Wilson, A. M., Shulgina, T., Kawzenuk, B., Sellars, S., Rutz, J. J., et al. (2019). ARTMIP-Early start comparison of atmospheric river detection tools: How many atmospheric rivers hit northern California’s Russian River watershed? *Climate Dynamics*, 52(7), 4973–4994. <https://doi.org/10.1007/s00382-018-4427-5>
- Rutz, J. J., Shields, C. A., Lora, J. M., Payne, A. E., Guan, B., Ullrich, P., et al. (2019). The atmospheric river tracking method intercomparison project (ARTMIP): Quantifying uncertainties in atmospheric river climatology. *Journal of Geophysical Research: Atmospheres*, 124(24), 13777–13802. <https://doi.org/10.1029/2019JD030936>
- Rutz, J. J., Steenburgh, W. J., & Ralph, F. M. (2014). Climatological characteristics of atmospheric rivers and their inland penetration over the western United States. *Monthly Weather Review*, 142(2), 905–921. <https://doi.org/10.1175/MWR-D-13-00168.1>
- Shields, C. A., Rutz, J. J., Leung, L.-Y., Ralph, F. M., Wehner, M., Kawzenuk, B., et al. (2018). Atmospheric river tracking method intercomparison project (ARTMIP): Project goals and experimental design. *Geoscientific Model Development*, 11(6), 2455–2474. <https://doi.org/10.5194/gmd-11-2455-2018>
- Simpson, I. R., Hitchcock, P., Shepherd, T. G., & Scinocca, J. F. (2011). Stratospheric variability and tropospheric annular-mode timescales. *Geophysical Research Letters*, 38(20), L20806. <https://doi.org/10.1029/2011GL049304>
- Son, S.-W., Kim, H., Song, K., Kim, S.-W., Martineau, P., Hyun, Y.-K., & Kim, Y. (2020). Extratropical prediction skill of the subseasonal-to-seasonal (S2S) prediction models. *Journal of Geophysical Research: Atmospheres*, 125(4), e2019JD031273. <https://doi.org/10.1029/2019JD031273>
- Thompson, D. W., Baldwin, M. P., & Wallace, J. M. (2002). Stratospheric connection to Northern Hemisphere wintertime weather: Implications for prediction. *Journal of Climate*, 15(12), 1421–1428. [https://doi.org/10.1175/1520-0442\(2002\)015<1421:SCTNHW>2.0.CO;2](https://doi.org/10.1175/1520-0442(2002)015<1421:SCTNHW>2.0.CO;2)
- Toride, K., & Hakim, G. J. (2021). Influence of low-frequency PNA variability on MJO teleconnections to North American atmospheric river activity. *Geophysical Research Letters*, 48(13), e2021GL094078. <https://doi.org/10.1029/2021GL094078>
- Tripathi, O. P., Charlton-Perez, A., Sigmond, M., & Vitart, F. (2015). Enhanced long-range forecast skill in boreal winter following stratospheric strong vortex conditions. *Environmental Research Letters*, 10(10), 104007. <https://doi.org/10.1088/1748-9326/10/10/104007>
- Waliser, D., & Guan, B. (2017). Extreme winds and precipitation during landfall of atmospheric rivers. *Nature Geoscience*, 10(3), 179–183. <https://doi.org/10.1038/ngeo2894>
- White, C. J., Carlsen, H., Robertson, A. W., Klein, R. J., Lazo, J. K., Kumar, A., et al. (2017). Potential applications of subseasonal-to-seasonal (S2S) predictions. *Meteorological Applications*, 24(3), 315–325. <https://doi.org/10.1002/met.1654>
- White, C. J., Domeisen, D. I., Acharya, N., Adefisan, E. A., Anderson, M. L., Aura, S., et al. (2022). Advances in the application and utility of subseasonal-to-seasonal predictions. *Bulletin of the American Meteorological Society*, 103(6), E1448–E1472. <https://doi.org/10.1175/BAMS-D-20-0224.1>
- Wilks, D. (2016). “The stippling shows statistically significant grid points”: How research results are routinely overstated and overinterpreted, and what to do about it. *Bulletin of the American Meteorological Society*, 97(12), 2263–2273. <https://doi.org/10.1175/BAMS-D-15-00267.1>
- Woollings, T., Barnes, E., Hoskins, B., Kwon, Y.-O., Lee, R. W., Li, C., et al. (2018). Daily to decadal modulation of jet variability. *Journal of Climate*, 31(4), 1297–1314. <https://doi.org/10.1175/JCLI-D-17-0286.1>
- Woollings, T., Hannachi, A., & Hoskins, B. (2010). Variability of the North Atlantic eddy-driven jet stream. *Quarterly Journal of the Royal Meteorological Society*, 136(649), 856–868. <https://doi.org/10.1002/qj.625>
- Zhang, J., Zheng, H., Xu, M., Yin, Q., Zhao, S., Tian, W., & Yang, Z. (2022). Impacts of stratospheric polar vortex changes on wintertime precipitation over the Northern Hemisphere. *Climate Dynamics*, 58(11–12), 1–17. <https://doi.org/10.1007/s00382-021-06088-x>

- Zhou, Y., O'Brien, T. A., Ullrich, P. A., Collins, W. D., Patricola, C. M., & Rhoades, A. M. (2021). Uncertainties in atmospheric river lifecycles by detection algorithms: Climatology and variability. *Journal of Geophysical Research: Atmospheres*, *126*(8), e2020JD033711. <https://doi.org/10.1029/2020JD033711>
- Zhu, Y., & Newell, R. E. (1994). Atmospheric rivers and bombs. *Geophysical Research Letters*, *21*(18), 1999–2002. <https://doi.org/10.1029/94GL01710>
- Zhu, Y., & Newell, R. E. (1998). A proposed algorithm for moisture fluxes from atmospheric rivers. *Monthly Weather Review*, *126*(3), 725–735. [https://doi.org/10.1175/1520-0493\(1998\)126<0725:APAFMF>2.0.CO;2](https://doi.org/10.1175/1520-0493(1998)126<0725:APAFMF>2.0.CO;2)

Erratum

In the previously published version of this article, two typographical errors appeared in the caption of Figure 5. The part label “(e)” was incorrectly replaced with a second label “(c),” and “(c and d)” should have read “(c–d).” These errors have since been corrected, and the present version may be considered the authoritative version of record.